# Doppler interference in dissociative resonant photoemission

| | |
|---|---|
| 著者 | Baev A., Gel'mukhanov F., Salek P., Agren H., Ueda K., Fanis A. de, Okada K., Sorensen S. |
| journal or publication title | Physical Review. A |
| volume | 66 |
| number | 2 |
| page range | 022509 |
| year | 2002 |
| URL | http://hdl.handle.net/10097/53548 |

doi: 10.1103/PhysRevA.66.022509

# Doppler interference in dissociative resonant photoemission

A. Baev,[1] F. Gel'mukhanov,[1,*] P. Sałek,[1] H. Ågren,[1] K. Ueda,[2] A. de Fanis,[2] K. Okada,[3] and S. Sorensen[4]
[1]*Theoretical Chemistry, Royal Institute of Technology, SCFAB, S-10691 Stockholm, Sweden*
[2]*Institute of Multidisciplinary Research for Advanced Materials, Tohoku University, Sendai 980-8577, Japan*
[3]*Department of Chemistry, Hiroshima University, Higashi-Hiroshima 739-8526, Japan*
[4]*Department of Synchrotron Radiation Research, Institute of Physics, University of Lund, Box 118, S-221 00 Lund, Sweden*
(Received 1 April 2002; published 30 August 2002)

Resonant photoemission involving dissociative core excited states has been the subject of a great number of experimental and theoretical investigations in recent time. The resonant decay of such dissociating systems has been shown to lead to semiatomic Auger electron emission spectra, with particular angular behavior. In the present paper a detailed theoretical analysis of dissociative resonant photoemission spectra of *homonuclear* diatomic molecules is presented. The theory addresses both fixed in space and randomly oriented homonuclear molecules and emphasizes the Doppler effect and the role of the interference between channels referring to the Doppler split atomic fragments. It is shown that peaks originating from decay in the atomic fragments can be asymmetric and structured due to the Doppler interference effect. The predicted strong non-Lorentzian behavior of the substructure on the top of the Doppler broadened atomiclike contribution is traced to the interplay between decay channels leading to gerade and ungerade final states. Simulations based on wave-packet theory are compared with experimental data for molecular oxygen. Our numerical simulations of the atomiclike resonance of fixed in space molecules show that the spectral profile is very sensitive to the shape of interatomic potentials of core excited and final states. It is shown that the Doppler effect in the decay spectra depends upon the symmetry of the core excited state.

DOI: 10.1103/PhysRevA.66.022509 PACS number(s): 33.20.Rm, 33.80.Gj, 33.70.−w

## I. INTRODUCTION

Channel-channel interference is a highly observable effect inherent in x-ray scattering spectroscopies of species possessing short-lived inner-shell hole states. When the lifetime broadening is of the same order of magnitude as the level splitting the decay channels referring to the different levels will interfere. The interference not only distorts the spectrum but can also modify the center of gravity of the vertical transitions shifting the apparent binding energies. Ever since the first prediction of lifetime vibrational interference in vibrationally resolved x-ray emission spectra [1], the interference effect has been analyzed and measured in many different circumstances [2–5].

These measurements are possible mainly as a consequence of modern synchrotron radiation sources providing high-resolution soft x-rays. Detailed studies of interference as manifested in *resonant* x-ray spectroscopies, such as x-ray resonant photoemission (RPE) and radiative x-ray Raman scattering spectroscopy, require tunable narrow-band radiation. For dissociative intermediate core excited states, resonant dissociative photoemission or fluorescence spectroscopies have revealed particularly interesting scattering spectra motivating theoretical interpretations such as interference. A large number of fundamental and applied studies have been presented in this field [3,5–12]. An excellent example of the important exchange between theoretical work and experiment is the prediction and verification of atomic holes, which is a manifestation of interference between nuclear continua belonging to the molecular compound and the atomic fragment from resonant photoemission decay [13–15].

Quite recently it was predicted that RPE from dissociative core excited states can be strongly influenced by the electronic Doppler effect, and that the resonance related to a decay transition in a fragment of dissociation (atomiclike resonance) can be ''Doppler'' split [16]. This effect was observed for oxygen [17,18] and recently also for ozone [19], HF [20], and $SF_6$ [21]. The electronic Doppler effect can be observed also in molecular bands in the spectral region related to the transitions between parallel parts of the core excited and final state potentials [22]. When the decay transitions appear between bound states, the center of gravity of the RPE profile can be Doppler shifted [23]. The electronic Doppler effect makes the electron-ion coincidence spectrum of homonuclear molecules [24] asymmetrical. It was also predicted that the additional structure of so-called ''atomiclike'' peaks can be manifested as a substructure on the top of the broad Doppler peak [16,17,23], which refers to a new kind of interference effect, a *Doppler interference* effect. This substructure can in principle be sharper than both the lifetime broadening and the width of the spectral functions of the x-ray excitation (resonance ultranarrowing).

The examples mentioned above highlight some of the many possibilities to analyze new physical effects which are offered by current synchrotron-based spectroscopies in connection with resonant scattering channels for dissociative core excited states. In the present work we focus on the effect of *Doppler interference*, namely the role of the interference effect between the Doppler split homonuclear species, and analyze in detail the origin of the structures in the final-state spectrum.

*Permanent address: Institute of Automation and Electrometry, 630090 Novosibirsk, Russia.

 

Our analysis is focused on the spectral shape and broadening of the atomiclike resonances. The naive picture says that these resonances have a Lorentzian shape with the width equal to the lifetime broadening. First of all we confirm earlier findings [16] that the atomiclike resonance can be Doppler split (parallel geometry) or Doppler broadened (perpendicular geometry). We predict also an asymmetry and additional broadening of the atomiclike resonance caused by the finite lifetime of the core excited state in the sense that the decay events take place between slightly nonparallel potential curves because the nuclear wave packet has no time to reach the ''strict'' region of dissociation. We find that the shape of the atomiclike resonance of aligned molecules is related to the shape of interatomic potentials. This makes RPE spectroscopy of atomic transitions of fixed in space molecules very promising for studies of interatomic potentials, something that now is a realistic proposition owing to the developments of energy resolved ion-electron coincidence techniques [25]. Simulations are carried out with the aid of wave-packet techniques applied to the GS$-$O $1s\sigma^{*}-2\sigma_g^{-1}/2\sigma_u^{-1}$ resonant photoemission transition in molecular oxygen in order to illustrate various aspects of the theoretical analysis. A comparison with a recently recorded RPE spectrum of $O_2$ is made and discussed.

## II. TIME-INDEPENDENT DESCRIPTION OF RESONANT PHOTOEMISSION FROM HOMONUCLEAR DIATOMICS

The role of the Doppler effect and interchannel interference on the formation of the RPE profile can be clearly understood in the framework of the stationary formalism, as we briefly describe below.

### The localized picture of scattering

We consider the situation when a molecule absorbs an x-ray photon of frequency $\omega$ followed by a Coulomb triggered decay to a set of final states which produces an Auger electron of energy $E$. When the incident x-ray beam is monochromatic the spectral features of the RPE process can be described by the double differential cross section:

$$\sigma_0(E,\omega)=\sum_f |F_f|^2\Delta(\omega-E-\omega_{f0},\Gamma_f), \tag{1}$$

where $\Gamma_f$ is the lifetime broadening of the final state $f$. In the localized picture resonant scattering of x-ray photons by homonuclear diatomic molecules goes through intermediate states with a core hole localized at one of the two atoms, $n=1, 2$. These scattering channels are indistinguishable, and the scattering amplitude is therefore the sum of two contributions

$$F_f=F_f^{(1)}+F_f^{(2)}, \quad F_f^{(n)}=-\imath\langle\Psi_f|\Psi_f^{(n)}(0)\rangle,$$

$$\Psi_f^{(n)}(0)=\imath\sum_c \frac{Q_{fc}^{(n)}|c\rangle\langle c|\mathcal{D}_{c0}^{(n)}|0\rangle}{\omega-\omega_{c0}+\imath\Gamma}, \quad \mathcal{D}_{c0}^{(n)}=\mathbf{e}\cdot\mathbf{D}_{c0}^{(n)}. \tag{2}$$

Here $\mathbf{e}$ is the polarization vector of the x-ray photon, $\mathbf{D}_{c0}^{(n)}$ is the dipole matrix element between core excited and ground electronic states, $\omega_{c0}=E_c-E_0$ is the resonant frequency of core excitation $0\rightarrow c$, and $\Gamma$ is the inverse lifetime of the core excited state. The scattering amplitude is written in the Born-Oppenheimer approximation with $|0\rangle$, $|c\rangle$, and $|\Psi_f\rangle$ as nuclear wave functions of the ground, core excited, and final states, respectively. To be specific, we consider here the case of K excitation. Due to strong localization of the $1s_n$ function, only a region near the $n$th atom with the coordinate $\mathbf{R}_n$ is important for the decay amplitude $Q_{fc}^{(n)}$. The wave function of the fast Auger electron with the momentum $\mathbf{k}$ reads in this region

$$\Psi_{\mathbf{k}}(\mathbf{r})\approx\psi_{\mathbf{k}}(\mathbf{r}_n)e^{\imath\mathbf{k}\cdot\mathbf{R}_n},$$

$$\psi_{\mathbf{k}}(\mathbf{r}_n)\approx\sum_{lm} R_{kl}(r_n)Y_{lm}(\hat{\mathbf{r}}_n). \tag{3}$$

Here $\mathbf{r}_n=\mathbf{r}-\mathbf{R}_n$, $Y_{lm}(\hat{\mathbf{r}}_n)$ are the spherical functions, $\hat{\mathbf{r}}=\mathbf{r}/r$. This gives us a phase factor in the Coulomb matrix element. Let us put the origin in the center of gravity of the molecule, where $\mathbf{R}_1=-\mathbf{R}/2$, $\mathbf{R}_2=\mathbf{R}/2$, and

$$Q_{fc}^{(1)}=q_{fc}^{(1)}e^{-\imath\mathbf{k}\cdot\mathbf{R}/2}, \quad Q_{fc}^{(2)}=q_{fc}^{(2)}e^{\imath\mathbf{k}\cdot\mathbf{R}/2}. \tag{4}$$

First of all, such phase factors in the electronic matrix elements result in phase factors in the partial scattering amplitudes [16]

$$F_f^{(1)}=\mathcal{F}_f^{(1)}e^{-\imath qR_0}, \quad F_f^{(2)}=\mathcal{F}_f^{(2)}e^{\imath qR_0},$$

$$q=\frac{1}{2}k\cos\theta, \tag{5}$$

where $R_0$ is the equilibrium internuclear distance, and $\theta$ is the angle between the momentum $\mathbf{k}$ of an Auger electron and the molecular axis.

Another important manifestation of the phase factors (4) is the electronic Doppler effect for the case of dissociative core excited states. When the scattering duration time [26] is large the nuclear wave packet can reach the region of dissociation, leading to decay events that take place in both the ''molecular'' and in the ''dissociative'' regions. These decay transitions form a broad ''molecular'' background and narrow atomiclike peaks [3]. The corresponding scattering amplitude thus consists of molecular and atomic contributions.

$$\mathcal{F}_f^{(n)}=\mathcal{F}_f^{(n)}(\mathrm{mol})+\frac{q_{fc}^{(n)}(\infty)\mathcal{D}_{c0}^{(n)}}{E-\omega_{cf}(\infty)\pm kv\cos\theta+\imath\Gamma},$$

$$v=\sqrt{\frac{\Delta\epsilon}{2\mu}}, \tag{6}$$

where $\omega_{cf}(\infty)=U_c(\infty)-U_f(\infty)$, and $q_{fc}(\infty)$ is the decay resonant frequency, and the decay matrix element, respectively; label $\infty$ specifies that the corresponding quantity is given for the dissociation region, $R=\infty$. Here we used the energy conservation law for the whole scattering process.

The free motion of the dissociating atoms leads to the electronic Doppler shift $\mathbf{k}\cdot\mathbf{v}$ which has opposite sign (+ and −) for atoms 1 and 2. The speed $v$, of a dissociating atom of a molecule is expressed via the kinetic energy release, $\Delta\epsilon = \omega + E_0 - U_c(\infty)$, in the dissociative intermediate state.

In the general case two scattering channels, $n=1$ and 2, [Eq. (6)] interfere

$$\sigma(E,\omega) = \sum_{f=g,u} [|\mathcal{F}_f^{(1)}|^2 + |\mathcal{F}_f^{(2)}|^2 + 2\,\mathrm{Re}(\mathcal{F}_f^{(1)*}\mathcal{F}_f^{(2)} e^{\iota k R_0 \cos\theta})]\Delta(\omega - E - \omega_{f0}, \Gamma_f). \tag{7}$$

This interference will be suppressed $\mathcal{F}_f^{(1)*}\mathcal{F}_f^{(2)} \approx 0$ when the Auger electron is emitted along the molecular axis and $kv \gtrsim \Gamma$ since the scattering channels are distinguishable. The Doppler splitting is equal to zero when $\mathbf{k} \perp \mathbf{R}$. In this case the scattering channels are indistinguishable and the interference reaches a maximum.

However, the additional mechanism of suppression of the interference exists. In the region of dissociation one cannot distinguish gerade and ungerade final states of equal energy. Due to this fact both gerade and ungerade partial cross sections contribute to the same atomic peak although the gerade and ungerade interference terms have opposite signs [16]. It may seem that these terms would cancel each other, however, we show in Secs. IV and V that this cancellation is not complete due to different magnitudes of the gerade and ungerade interference terms (see also [16]).

The discussion thus far only concerns aligned molecules in the sample. Molecules are randomly oriented in the gas phase and the RPE cross section has then to be averaged over the molecular orientations. We outline this averaging in Sec. III A. It is worth noting that even for randomly oriented molecules one can speak about certain molecular orientations due to the orientational selectivity of photoabsorption, which depends on the angle between the polarization vector and the transition dipole moment (2).

## III. WAVE-PACKET DYNAMICS

It appears to be useful both from theoretical and computational points of view to switch to the time-dependent representation for the RPE cross section (1). This is accomplished with the aid of a half-Fourier transform of the scattering amplitude (2)

$$\sigma_0(E,\omega) = \frac{1}{\pi}\mathrm{Re}\int_0^\infty d\tau \sigma_0(\tau) e^{\iota(\omega - E + E_0)\tau}. \tag{8}$$

The impossibility of distinguishing between scattering channels through equivalent atoms makes the autocorrelation function $\sigma_0(\tau)$ for a homonuclear molecule

$$\sigma_0(\tau) = \sum_{f=g,u} [\sigma_f^{(1)}(\tau) + \sigma_f^{(2)}(\tau) + \sigma_f^{(12)}(\tau)],$$
$$\sigma_f^{(n)}(\tau) = \langle \Psi_f^{(n)}(0) | \Psi_f^{(n)}(\tau)\rangle, \tag{9}$$
$$\sigma_f^{(12)}(\tau) = \langle \Psi_f^{(1)}(0) | \Psi_f^{(2)}(\tau)\rangle + \langle \Psi_f^{(2)}(0) | \Psi_f^{(1)}(\tau)\rangle,$$

qualitatively different from the case of a heteronuclear molecule [3,16]. Indeed, besides the direct terms $\sigma_f^{(1)}(\tau)$ and $\sigma_f^{(2)}(\tau)$, the autocorrelation function also includes an interference term $\sigma_f^{(12)}(\tau)$. The autocorrelation functions are given by overlaps of the wave packets

$$\Psi_f^{(n)}(\tau) = e^{-(\iota H_f + \Gamma_f)\tau}\Psi_f^{(n)}(0),$$
$$\Psi_f^{(n)}(0) = \int_0^\infty dt e^{[\iota(\omega + E_0) - \Gamma]t} Q_{fc}^{(n)} \psi_c(t). \tag{10}$$

To find $\Psi_f^{(n)}(0)$ we have to solve the time-dependent Schrödinger equation for the wave packet $\psi_c(t) = \exp(-\iota H_c t)\mathcal{D}|0\rangle$ propagating in the core excited potential with the initial condition $\psi_c(0) = \mathcal{D}|0\rangle$. The next step is the solution to the time-dependent Schrödinger equation for the wave packet $\Psi_f^{(n)}(t)$ propagating along the final state potential surface.

As it was pointed out above (see also Ref. [16]) the opposite phases (4) of the partial scattering amplitudes (2) give the phase factor $\exp(\iota\mathbf{k}\cdot\mathbf{R})$ in the interference term $\sigma_f^{(12)}(\tau)$ [see also Eq. (7)] and the opposite Doppler shifts of the atomic peaks related to the atoms 1 and 2.

In real experiments the incident radiation has finite spectral width. The cross section in this case is given by the convolution of the cross section for monochromatic excitation $\sigma_0(E,\omega)$ with the spectral distribution $\Phi$ of incident radiation [3,13]

$$\sigma(E,\omega) = \int d\omega_1 \sigma_0(E,\omega_1)\Phi(\omega - \omega_1, \gamma). \tag{11}$$

### Averaging over molecular orientations. Orientational selectivity of photoexcitation

The RPE cross section for the randomly oriented sample must be [Eq. (11)] averaged over all molecular orientations $\hat{\mathbf{R}} = \mathbf{R}/R$. This procedure is equivalent to averaging over all directions of $\mathbf{e}$ and $\mathbf{k}$ with a fixed angle between $\mathbf{e}$ and $\mathbf{k}$.

The dependence of the RPE cross section on the direction of molecule axis, $\hat{\mathbf{R}}$, originates from the photoabsorption amplitude $\mathcal{D}_{c0} = \mathbf{e}\cdot\mathbf{D}_{c0}$, the decay amplitude $q_{fc} = q_{fc}(\theta)$, and the phase factors $\exp[\pm\iota(kR/2)\cos\theta]$. It is instructive to extract the photoabsorption factor from the RPE cross section

$$\sigma(E,\omega) = |\mathbf{e}\cdot\hat{\mathbf{D}}_{c0}|^2 \sigma'(E,\omega;\theta). \tag{12}$$

For example, $\sigma(E,\omega) = (|\mathbf{e}\cdot\hat{\mathbf{D}}_\pi^x|^2 + |\mathbf{e}\cdot\hat{\mathbf{D}}_\pi^y|^2)\sigma'(E,\omega;\theta)$ for $1s \to \pi^*$ photoabsorption transition ($\mathbf{D}_\pi \perp \mathbf{R}$), and $\sigma(E,\omega) = |\mathbf{e}\cdot\hat{\mathbf{R}}|^2\sigma'(E,\omega;\theta)$ for $1s \to \sigma^*$ photoexcitation. Finally, the orientational averaging of the cross section is reduced to the averaging only over angles $\theta$ between $\mathbf{k}$ and $\mathbf{R}$

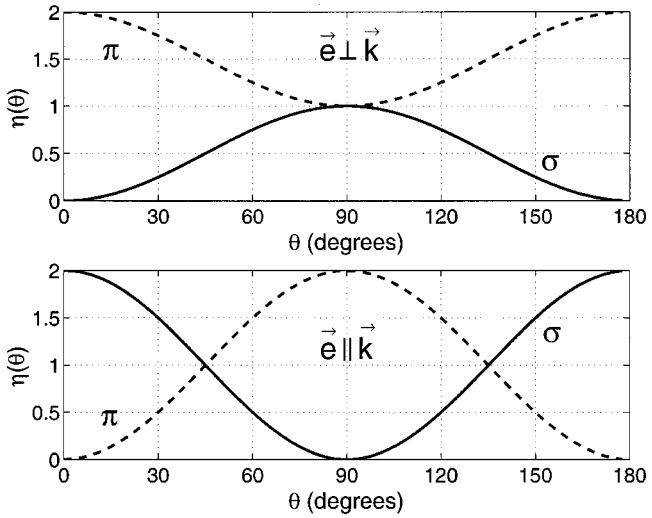


FIG. 1. Orientational selectivity of the photoabsorption (14) for $1s\rightarrow\sigma^*$ and $1s\rightarrow\pi^*$ photoexcitations.

$$\overline{\sigma}(E,\omega)=\frac{1}{4\pi}\int d\hat{\mathbf{R}}\sigma(E,\omega)$$

$$=\frac{1}{4}\int_0^{\pi} d\theta\sin\theta\sigma'(E,\omega;\theta)\eta(\theta). \tag{13}$$

For a fixed angle $\theta$ between **R** and **k** the angular distribution of core excited molecules depends both on $\theta$ and the angle between **e** and **k** (Fig. 1)

$$\eta(\theta)=\begin{cases}1+\cos^2\theta-(3\cos^2\theta-1)(\hat{\mathbf{e}}\cdot\hat{\mathbf{k}})^2,\\ 1s\rightarrow\pi^*,\\ 2\cos^2\theta+(3\cos^2\theta-1)[(\hat{\mathbf{e}}\cdot\hat{\mathbf{k}})^2-1],\\ 1s\rightarrow\sigma^*.\end{cases} \tag{14}$$

The orientational selectivity of photoexcitation, $\eta(\theta)$, descends from the averaging of $|\mathbf{e}\cdot\hat{\mathbf{D}}_{c0}|^2$, according to the equation: $\overline{e_ie_j}=\{\delta_{ij}[1-(\hat{\mathbf{e}}\cdot\hat{\mathbf{k}})^2]+\hat{k}_i\hat{k}_j[3(\hat{\mathbf{e}}\cdot\hat{\mathbf{k}})^2-1]\}/2$. Clearly, this selectivity is qualitatively different for $1s\rightarrow\pi^*$ and $1s\rightarrow\sigma^*$ excitations due to different orientations of $\pi$ and $\sigma$ orbitals relative to the molecular axis.

#### *1. Doppler splitting*

The Doppler shift $|\mathbf{k}\cdot\mathbf{v}|$, which is hidden in $\sigma'(E,\omega;\theta)$, takes a maximum value when $\theta=0°$ and 180°. This means that an ideal condition for observation of the Doppler splitting occurs if $\eta(\theta)$ is maximal for these angles. For the $1s\rightarrow\sigma^*$ channel it happens when $\mathbf{k}\|\mathbf{e}$, while for the $1s\rightarrow\pi^*$ excitation when $\mathbf{k}\perp\mathbf{e}$ (Fig. 1). Another distinction of $\sigma$ and $\pi$ excitations is the depth of the $\eta(\theta)$ function for $\theta=90°$ which defines the contrast of the Doppler splitting. Contrary to the $\sigma$ channel, the suppression of the $\eta(\theta)$ function for $\theta=90°$ is not complete in the case of $\pi$ excitation (Fig. 1).

#### *2. Doppler broadening*

The Doppler splitting is absent when $\mathbf{k}\perp\mathbf{e}$ ($\mathbf{k}\|\mathbf{e}$) for $\sigma$ ($\pi$) channels since here $\eta(0°)=\eta(180°)=0$ (Fig. 1). The atomic peak experiences then only the Doppler broadening, but the interference becomes important for such experimental geometries.

## IV. INTERFERENCE TERM

When $\mathbf{k}\perp\mathbf{e}$ the axes of the core excited molecules are oriented primarily perpendicularly to **k**. In this case the Doppler shift is small and the interference of the two scattering channels takes a maximum value. This interference yields the narrow structure (dip or peak) on the top of the atomiclike resonance [16]. We intend here to gain more physical insight into the nature of this interference structure. The main physical reason for this structure is the interplay of the Doppler shift $\mathbf{k}\cdot\mathbf{v}$, phase factor $\exp(\imath\mathbf{k}\cdot\mathbf{R})$, and orientational averaging.

### A. Role of symmetry

The parity of states is important for the interference term [16]. Let us analyze the parity sensitive factor in the scattering amplitude (2)

$$\zeta_f^{(n)}=q_{fc}^{(n)}D_{c0}^{(n)} \tag{15}$$

for the studied participator process in molecular oxygen:

$$1s\rightarrow\sigma^*\rightarrow[\sigma^*\rightarrow 1s;2\sigma_f\rightarrow\text{continuum}],$$

$$f=g,u. \tag{16}$$

In the molecular frame with $\mathbf{R}\|z$ we can write the following expansion of the molecular orbitals (MOs) over atomic orbitals: $2\sigma_f=\Sigma_n\Sigma_l c_{fl}^{(n)}R_l(r_n)Y_{l0}(\hat{\mathbf{r}}_\mathbf{n})$, $\sigma^*=\Sigma_n\Sigma_L C_{uL}^{(n)}R_L(r_n)Y_{L0}(\hat{\mathbf{r}}_\mathbf{n})$. The wave function of a fast Auger electron is given by Eq. (3).

This immediately results in

$$\zeta_f^{(n)}=\sum_L\sum_l\zeta_{f,Ll}^{(n)},\quad \zeta_{f,Ll}^{(n)}=c_{fl}^{(n)}(R)C_{u1}^{(n)}C_{uL}^{(n)}(R)\zeta_{f,Ll}, \tag{17}$$

where the parameter $\zeta_{f,Ll}$ is independent of the number of atoms *n*. To be specific let us assume that local frames for first and second atoms have the same orientation. The parity of MOs $[c_{gl}^{(2)}=(-1)^l c_{gl}^{(1)}, c_{ul}^{(2)}=-(-1)^l c_{ul}^{(1)}]$ leads to

$$\zeta_{g,Ll}^{(2)}=-(-1)^{L+1}\zeta_{g,Ll}^{(1)},\quad \zeta_{u,Ll}^{(2)}=(-1)^{L+l}\zeta_{u,Ll}^{(1)}, \tag{18}$$

respectively. We arrived at the important conclusion that gerade and ungerade final states have opposite signs of the interference contributions

$$\zeta_{g,Ll}^{(2)}\zeta_{g,Ll}^{(1)*}=-(-1)^{L+l}|\zeta_{g,Ll}^{(1)}|^2,$$
$$\zeta_{u,Ll}^{(2)}\zeta_{u,Ll}^{(1)*}=(-1)^{L+l}|\zeta_{u,Ll}^{(1)}|^2. \tag{19}$$

It is also important to note that the decay amplitude depends on the internuclear distance, $q_{fc}^{(n)}(R)$, contrary to the photoabsorption amplitude $D_{c0}^{(n)}$ which depends only on equilibrium distance, $R_0$. Due to this fact the MO coefficients in

Eq. (17) $c_{fl}^{(n)}(R)$ and $C_{uL}^{(n)}(R)$ depend on $R$, while $C_{u1}^{(n)} = C_{u1}^{(n)}(R_0)$. We will see now that the $R$ dependence of MO coefficients is very important for the interference term since these coefficients show the contribution of atomic orbitals (AOs) of different parities to the molecular orbital. Now we are at the stage to write down the final expression for the partial interference contribution (9)

$$
\begin{aligned}
&[\sigma_g^{(12)}(\tau)+\sigma_u^{(12)}(\tau)]_{Ll} \\
&\quad=(-1)^{L+l}[\langle\overline{\Psi}_u^{(1)}(0)||\zeta_{u,Ll}^{(1)}|^2|\overline{\Psi}_u^{(2)}(\tau)\rangle \\
&\quad+\langle\overline{\Psi}_u^{(2)}(0)||\zeta_{u,Ll}^{(1)}|^2|\overline{\Psi}_u^{(1)}(\tau)\rangle \\
&\quad-\langle\overline{\Psi}_g^{(1)}(0)||\zeta_{g,Ll}^{(1)}|^2|\overline{\Psi}_g^{(2)}(\tau)\rangle \\
&\quad-\langle\overline{\Psi}_g^{(2)}(0)||\zeta_{g,Ll}^{(1)}|^2|\overline{\Psi}_g^{(1)}(\tau)\rangle].
\end{aligned}
\tag{20}
$$

Here the wave packets $\overline{\Psi}_f^{(n)}(\tau)$ is given by the same formula as $\Psi_f^{(n)}(\tau)$ with $\zeta_f^{(n)}=1$. As is well established now [27], the interchannel interference is strongly related to the parity selection rule for radiative x-ray Raman scattering. In the case of RPE we can speak about parity selection rules only when AOs of the same parity form MOs (it is the case of $\pi$ orbitals [28] or transitions in the dissociative region, Sec. V). The interference contributions for gerade and ungerade final states have the same absolute values only in the dissociative region: $\zeta_{g,Ll}^{(2)}\zeta_{g,Ll}^{(1)*}=-\zeta_{u,Ll}^{(2)}\zeta_{u,Ll}^{(1)*}=-(-1)^{L+l}|\zeta_{u,Ll}^{(1)}|^2$. For example, for oxygen, $c_{fl}^{(1)}=\delta_{l,1}/\sqrt{2}$, $C_{uL}^{(1)}=\delta_{L,1}/\sqrt{2}$ in the dissociative region, where only $p$ atomic orbitals contribute to MOs of the studied core excited and final states. This means that the interference contribution disappears if the dissociative contribution dominates in integrals (20) since in the region of dissociation

$$
\zeta_{g,Ll}^{(2)}\zeta_{g,Ll}^{(1)*}+\zeta_{u,Ll}^{(2)}\zeta_{u,Ll}^{(1)*}=|\zeta_{u,Ll}^{(1)}|^2-|\zeta_{g,Ll}^{(1)}|^2=0,
\qquad R\to\infty. \tag{21}
$$

The interference term (20) is different from zero only in the molecular region [where $|\zeta_u^{(1)}|^2-|\zeta_g^{(1)}|^2\neq 0$ is important in the matrix elements (20)]. Indeed in this region, the $2s$ atomic orbitals also contribute to $\sigma^*\equiv 3\sigma_u$ and $2\sigma_f$ MOs and the MO coefficients $C_{gL}^{(n)}(R)$ and $C_{uL}^{(n)}(R)$ become different for $2\sigma_g$ and $2\sigma_u$ orbitals. Equation (20) shows that the sign of the interference contribution strongly depends on the sign of $|\zeta_{u,Ll}^{(1)}|^2-|\zeta_{g,Ll}^{(1)}|^2$.

At first glance, Eq. (20) says that the total interference term disappears even in the molecular region if $|\zeta_{u,Ll}^{(1)}|^2-|\zeta_{g,Ll}^{(1)}|^2=0$. However, we will show in Sec. IV B that such a naive picture does not hold since $\overline{\Psi}_u^{(n)}(\tau)\neq\overline{\Psi}_g^{(n)}(\tau)$ due to different potentials of the ungerade and gerade final states.

We see, finally, that the interference contribution strongly depends on the relative contribution of molecular and dissociative regions to the integrals over nuclear separation, $R$, appearing in the matrix elements (20). Fortunately we can manipulate the molecular and dissociative contributions in these matrix elements by changing the duration time of the scattering process [3,26].

### B. The role of the scattering duration time

It is notable that in real situations scattering in both molecular and dissociative regions form atomic peaks (see Sec. V), and that the role of the molecular region is important for the interference term. We investigated above the role of the $R$ dependence of the electronic matrix elements $\zeta_f^{(n)}$ on the interference term (20). Now we intend to study another physical mechanism which gives a nonzero value of the interference term. To distinguish this mechanism from the previous one, we will assume here that the electronic matrix elements are the same for both gerade and ungerade final states:

$$
\zeta_{f,Ll}^{(n)}=1. \tag{22}
$$

As was pointed out earlier [16] the interference term and the RPE fine structure related to this term strongly depend on the lifetime broadening of the core excited state $\Gamma$. It is important to understand the dependence of the interference contribution on the duration of scattering [26]

$$
T=\frac{1}{\sqrt{\Omega^2+\Gamma^2}}, \tag{23}
$$

which is the function of $\Gamma$ and detuning $\Omega$.

#### *1. Role of lifetime broadening*

We keep in mind that the scattering amplitude (2) is a projection of the wave packet $\Psi_f^{(n)}(0)$ (10) on the final state $\Psi_f$. In the dissociative region the wave functions of gerade and ungerade final states normalized to the momentum have free-particle asymptotes ($f=g,u$)

$$
\Psi_f\approx\frac{1}{\sqrt{2\pi}}e^{\imath pR+\delta_f}, \quad p=\sqrt{2\mu\Delta\epsilon} \tag{24}
$$

with different phase shifts, $\delta_g\neq\delta_u$, due to different final state potentials $U_g(R)\neq U_u(R)$. Clearly, the strict continuum wave function, $\Psi_i$, is normalized to the $\delta$ function of momentum due to the dominant role of the plane wave asymptote on the norm of $\Psi_i$. Now we can rewrite the contribution of the wave packet propagating in the ungerade final state to the total cross section as follows:

$$
\begin{aligned}
\langle\Psi_u|\Psi_f^{(n)}(0)\rangle&=e^{\imath\delta}\langle\Psi_g|\Psi_f^{(n)}(0)\rangle \\
&\quad+\langle(\Psi_u-\Psi_g e^{\imath\delta})|\Psi_f^{(n)}(0)\rangle, \\
\delta&=\delta_u-\delta_g.
\end{aligned}
\tag{25}
$$

To provide some physical insight let us utilize simplified interatomic potentials for gerade and ungerade final states [29], see Fig. 2. The continuum wave functions $\Psi_g$ and $\Psi_u$ spanning over the potential step (gerade state) and the poten-

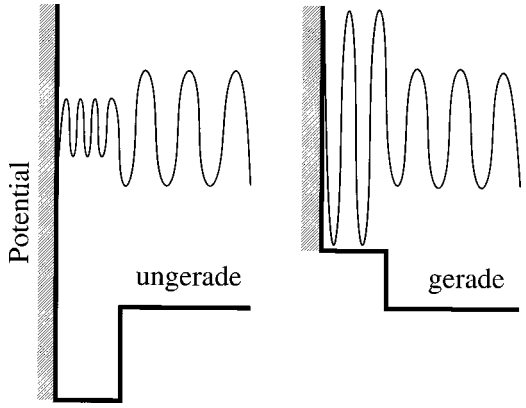


FIG. 2. Qualitative picture of ungerade and gerade molecular wave functions for corresponding model final state potentials. Illustration of the formation of the interference term for a finite lifetime of the core excited state.

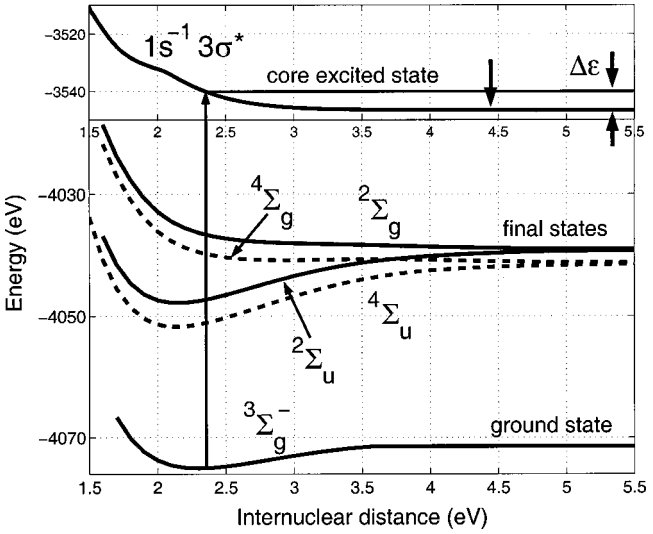


FIG. 3. Potential surfaces of the ground, core excited, and final states. Upper single arrow shows the region reached by a wave packet in the core excited state for $\Gamma=0.08$ eV and $\Omega=0$ [see Eq. (28)].

tial well (ungerade state) have the same amplitude in the dissociative region and different amplitudes in the molecular region (Fig. 2). Due to this one can expect different scattering amplitudes for gerade and ungerade final states (2), $F_g \neq F_u$, if the scattering duration is short and therefore only the molecular region contributes to the overlap (2). We then also expect that $F_g=F_u$ when $T\to\infty$ due to a major contribution of the dissociative region. However, our simulations show that this naive picture is valid only when we change $T$ by changing only $\Gamma$ with $\Omega=\text{const}$.

#### *2. Role of the detuning*

We found that in the dissociative region the ratio $|F_g/F_u|$ is nearly independent of the detuning $\Omega$. The reason for this is the spatial distribution of the wave packet [26] [which is denoted in Ref. [26] as $\Psi_T(\infty)$] that in the dissociative region behaves as

$$\Psi_f(0)\propto\exp\left(\frac{-2\Gamma(R-R_0)}{v}\right). \tag{26}$$

This equation shows that the spatial distribution of $\Psi_f(0)$ does not depend on detuning [increasing $|\Omega|$ only decreases the amplitude of $\Psi_f(0)$]. Due to this fact the overlap $\langle\Psi_f|\Psi_f^{(n)}\rangle$ (2) is the same for $f=g$ and $f=u$ for different $\Omega$ and the same $\Gamma$. The only role of the detuning is the suppression of both gerade and ungerade scattering channels by the same factor. Apparently, the role of the detuning becomes important when $|\zeta_u^{(1)}|^2-|\zeta_g^{(1)}|^2\neq 0$.

## V. COMPUTATIONAL

### A. Dynamics and potential surfaces

We have imposed several simplifying assumptions in the simulations. First of all we neglect the $R$ dependence of the electronic matrix element and we assume that they are the same for gerade and ungerade final states (22). This $R$ dependence is, however, very important for the interference contribution within the molecular region. Indeed, according to Sec. IV A, the interference term strongly depends on the parities of atomic orbitals which form the corresponding MOs. Clearly, the MOs are formed by AOs of different parities. On the way from the dissociative to the molecular region the relative weights of different AOs change drastically. The main subject of this study, the atomic peak is, however, not very sensitive to these changes. In the calculation we also neglect the anisotropy of the decay electronic matrix elements $q_{fc}$, for the case where $\Gamma_f=0.01$ eV for monochromatic excitation.

We study the following participator RPE process for molecular oxygen

$$\omega+O_2\Rightarrow\left\{\begin{matrix}O_2^*(1s_1\to\sigma^*)\\ O_2^*(1s_2\to\sigma^*)\end{matrix}\right\}\Rightarrow O_2^+(2\sigma_{g,u}^{-1})+e^-. \tag{27}$$

The potential curves of the ground, core excited, and final states are shown in Fig. 3. The ground and final $2\sigma_g^{-1}/2\sigma_u^{-1}(^2\Sigma_g,{}^4\Sigma_g/{}^2\Sigma_u,{}^4\Sigma_u)$ states of $O_2$ were computed with the aid of the DALTON code [30] with complete active space MCSCF wave functions with a large extended basis set: aug-cc-pVTZ. The details of the calculations can be obtained from the authors upon request. For the potential surface of the core excited $|{}^3\Sigma^-\rangle=|1s^{-1}\sigma^*({}^2\Sigma^-)\rangle$ state we have employed the extensive CI calculation data of Kosugi *et al.*, which were produced in connection with their investigation of the NEXAFS spectrum of $O_2$ [31,32]. It is appropriate to note that the $1s\to\sigma^*$ excitation leads to two states $|1s^{-1}\sigma^*({}^2\Sigma^-)\rangle$ and $|1s^{-1}\sigma^*({}^4\Sigma^-)\rangle$ related to the doublet, ${}^2\Sigma^-$, and quartet, ${}^4\Sigma^-$, ion cores, respectively. The gap between these states [31,32] is 2.5 eV. The potential curves were used in the wave-packet calculations employing the RAM [33] program developed by one of the authors.

We study here the lower doublet core excited state which is the only excited state in our experiment. According to Fig. 3 one can expect two atomic peaks due to decay transitions to doublet and quartet final states with a spacing of 2.2 eV in

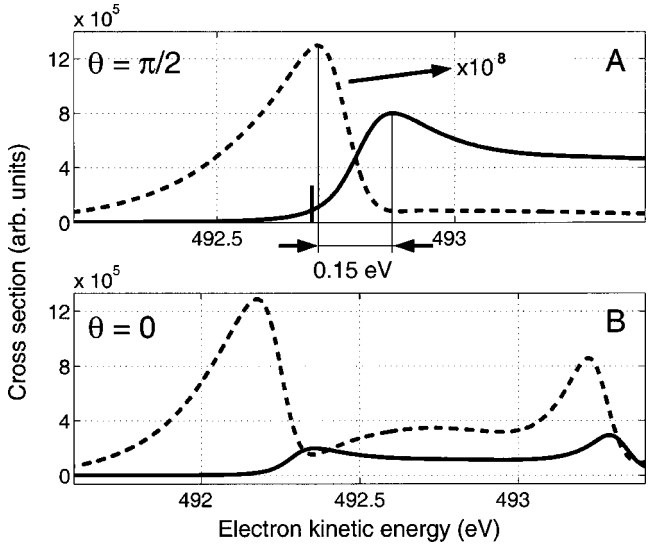


FIG. 4. Cross section for fixed in space orientation of oxygen. Gerade and ungerade final state contributions are shown with dashed and solid lines, respectively. $\Gamma=0.08$ eV. $\Omega=0$ eV. (A) $\mathbf{k}\perp\mathbf{R}$. The ''gerade'' atomic peak is almost completely suppressed due to parity selection rules. The stick shows the position of the atomic peak for $\Gamma=0$. (B) $\mathbf{k}\|\mathbf{R}$. The parity selection rules break down due to opposite Doppler shifts of the left-and right-propagating atoms.

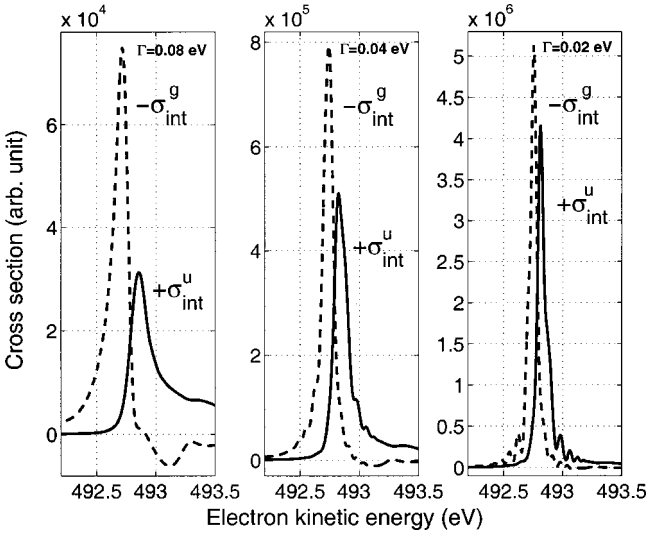


FIG. 5. Spectral distributions of the interference terms for the gerade and ungerade final states vs the lifetime broadening of the core excited state. $\Omega=0$.

the dissociation region, $R=\infty$, in agreement with the experimental photoelectron spectrum [34]. Experiment shows only one peak corresponding to the doublet final state which indicates a propensity that the spin multiplicity remains unchanged during the nonradiative decay. The propensity is, however, dependent on the actual coupling order as well as on the size of the matrix elements.

### B. Formation of spectrum of fixed in space molecule

Let us first analyze the RPE spectrum of fixed in space oxygen molecules (Fig. 4) with the molecular axis perpendicular and parallel to the direction of the Auger electron ejection and $\Omega=0$. When $\mathbf{R}\perp\mathbf{k}$ the Doppler shift is equal to zero. The well-defined parities of the core excited and final states, $L=l=1$, in the region of dissociation result in strict selection rules. This is due to the nonparallel potential surfaces in the region of the decay transition. The ''gerade'' contribution to the atomic peak is almost suppressed [Fig. 4(A)]. Such parity selection rules break down in the case of a parallel geometry [Fig. 4(B)] due to the opposite Doppler shifts of the left and right propagating atoms. One can see that both gerade and ungerade final states contribute to the Doppler split atomic peak in this case. The positions of the Doppler components for gerade and ungerade final states are different [see discussion of Eq. (29)]. It is worthwhile to note that such parity selection rules are absent in the general case for decay transitions in the molecular region where atomic orbitals with different parities ($L$, $l$) form the MOs. This is easy to see from the factor $(-1)^{L+l}$ in Eq. (20).

We see that the spectral profiles [Fig. 4(A)] for gerade and ungerade atomic peaks are asymmetric and are broader than the lifetime broadening. For example, the full width at half maximum (FWHM) of the gerade atomic peak ($\approx$0.2 eV) is larger than the lifetime broadening $2\Gamma=0.16$ eV. The main reason for this is that during the scattering $T=1/\Gamma$ the wave packet passes the distance

$$\Delta R\approx\frac{2v}{\Gamma}\sim 2 \quad \text{a.u.} \tag{28}$$

in the core excited state. As one can see from Fig. 3 this distance does not strictly reach the dissociative region, since the potential surfaces of final states and the core excited state are not parallel to each other. Moreover, gerade and ungerade final state are split, $\Delta U=U_u(R)-U_g(R)$, at the terminal point of the wave packet, $R=R_0+\Delta R$, which depends on the lifetime broadening according to Eq. (28). Figure 5 shows clearly that this splitting becomes smaller with increasing lifetime of the core excited state which agrees with Eq. (28). Indeed

$$\Delta U\approx 0.15,\ 0.08,\ 0.06 \ \text{eV} \tag{29}$$

for $\Gamma=0.08$, 0.04, 0.02 eV, respectively.

One can assume that the splitting $\Delta U$ also depends on the detuning $\Omega$ because $\Delta R\approx vT$ (28) depends on $\Omega$ through the scattering duration time (23). However, our simulations have shown very weak $\Omega$ dependence of $\Delta U$ and the energy position of the atomic peak.

We know that within the dissociative region the decay conserves the released kinetic energy $\Delta\epsilon_c=\Delta\epsilon_f$. Since the potential surfaces are not parallel near the quasiatomic region (28), the decay transitions with $\Delta\epsilon_c\neq\Delta\epsilon_f$ also contribute to the atomic peak. This results in broadening and asymmetry. The splitting (29) yields additional broadening of the total cross section. Numerical simulations (Sec. V) confirm this strong sensitivity of the shape of the atomic peak to the potential surfaces of core excited and final states [13].

### C. Analysis of the averaged cross sections

In the gas phase we have to average the cross section over molecular orientations according to Eq. (13). Now the Doppler shift is not equal to zero, yielding a Doppler broadening of the atomic peak. Another important role of the orientational averaging is the interplay of the phase factor $\exp(\imath kR_0 \cos\theta)$ (6) and the Doppler shift, $\pm kv\cos\theta$, in the interference term (7). This results in the narrow interference structure on top of the atomiclike peak with the width (FWHM) [16]

$$\Delta E = \frac{2D}{kR} = \frac{2v}{R} \sim 0.06 \text{ eV} \tag{30}$$

for a released energy of $\Delta\epsilon \approx 7.5$ eV and $R \approx 2.5$ a.u. Here $D = kv$ is the Doppler width. This is in agreement with the FWHM of the simulated profile ($\approx$0.06 eV) for a large core excited state lifetime broadening. $\Gamma = 0.02$ eV (Fig. 5). When the lifetime broadening decreases, $\Gamma = 0.08$ eV, the interference term becomes broader (FWHM$\approx$0.14 eV). The reason for this broadening is that the wave packet does not have time to reach the dissociative region for shorter lifetimes $1/\Gamma$, where all potential curves are parallel [see discussion of Fig. 4(A)]. Thus the finite $1/\Gamma$ violates Eq. (30) and gives the additional broadening of the interference term. Figure 5 shows this broadening clearly. We also see that the peak positions of the interference terms for gerade and ungerade final states are different [the spacing is approximately equal to 0.15 eV; the reason for this splitting was discussed above, see Eq. (29)]. The most important result of Fig. 5 is that the interference terms $\sigma^g_{\text{int}}$ and $\sigma^u_{\text{int}}$ for gerade and ungerade final states have opposite signs and the same absolute values for long-lived core excited states. This results in complete suppression of the interference contribution near the atomic peak, $\sigma_{\text{int}} = \sigma^g_{\text{int}} + \sigma^u_{\text{int}} = 0$, if $\Gamma = 0$ (see Sec. IV B). Due to this fact, the discussed above and here interference dip or peak on top of the atomic peak are absent for $\Gamma = 0$.

The final atomic spectral profile of oxygen is shown in Fig. 6(a). As far as we consider the core excitation to the $\sigma^*$ molecular orbital we will deal with transition dipole moments oriented along the molecular axis. It means that if the vectors of Auger electron momentum and radiation polarization are parallel (**k**$\|$**e**), we will see a dip in the middle of the averaged contour of the cross section, because the center corresponds to a perpendicular orientation of the momentum and molecular axis. This results in the Doppler splitting (2 kV$\approx$0.8 eV). In agreement with experimental data [17,18] this splitting is absent for perpendicular geometry (**k**$\perp$**e**). In this case the atomic peak is only Doppler broadened (FWHM$\approx$2 kV$\approx$0.8 eV). The comparison of the direct (dashed line) and total cross section (solid line) indicates that the narrow deep on the top of the Doppler broadened profile is caused only by the interference contribution. As it was discussed in Sec. IV A, the $R$ dependence of the electronic matrix elements can change the sign of the interference contribution. To mimic such a case we calculated the RPE profile of oxygen with the opposite sign of the interference term [Fig. 6(b)]. In this case the interchannel interference results in a narrow peak on the top of the Doppler broadened atomic peak.

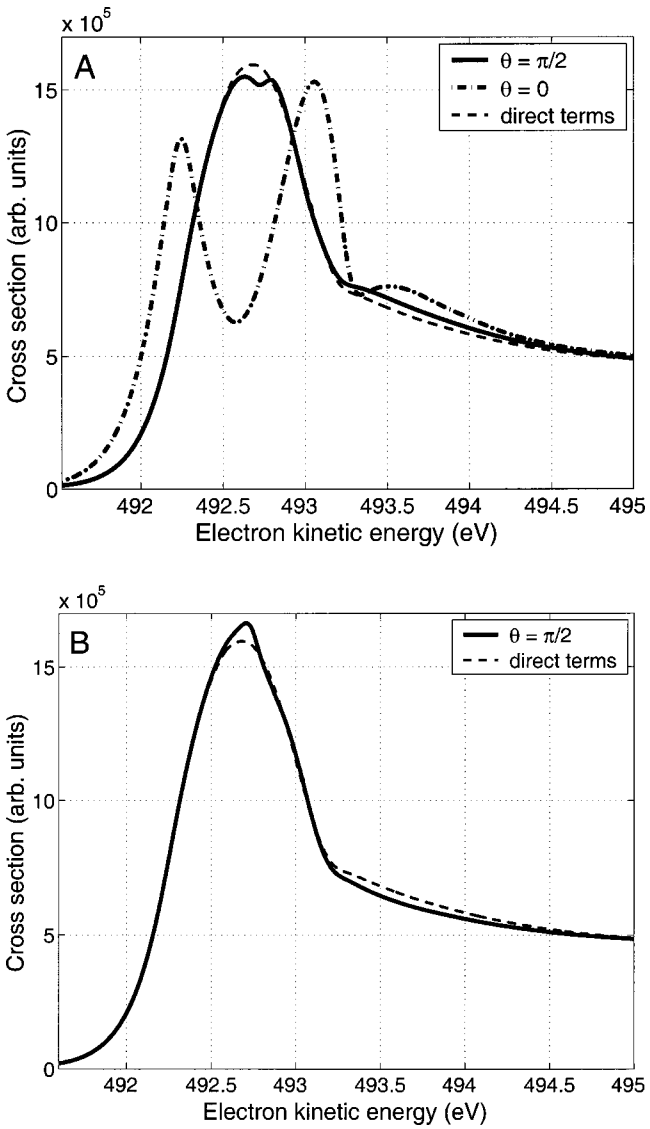


FIG. 6. (A) Averaged total cross section for different experimental geometries (**k**$\|$**e**: dot-dashed line, and **k**$\perp$**e**: solid line). The dashed line shows the total direct term for **k**$\perp$**e**. (B) The same except for an opposite sign of the interference term.

Figure 7 shows the RPE profile of oxygen over a broad spectral region. The high energy part of the spectrum shows the vibrational progression caused by the bound ungerade final state (continuum-bound transitions). The next peak is due to the continuum–continuum transitions in the molecular region. The last resonance is the atomic peak (also see the inset).

## VI. EXPERIMENT

The spectra were recorded at the undulator beamline 27SU [35] at SPring-8, Himeji, Japan. This beamline is equipped with a high-resolution, varied line spacing, plane grating monochromator [36]. The horizontal and vertical orientations of the **e** vector are chosen by using the first of the

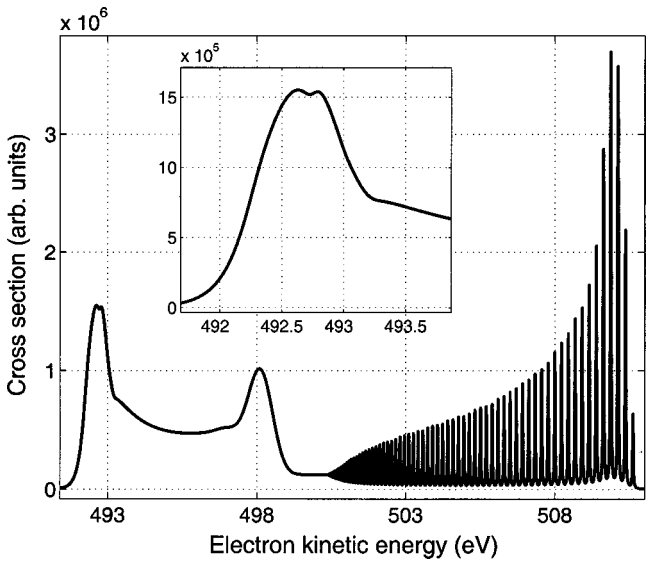


FIG. 7. Averaged total RPE cross section for $\mathbf{k}\perp\mathbf{e}$. $\Gamma=0.8$ eV. $\Omega=0$. The insert shows the atomic peak.

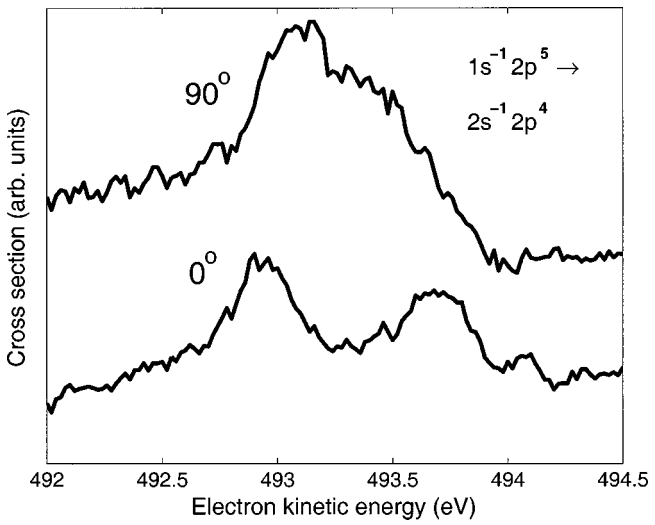


FIG. 8. Experimental spectra measured at 0° and 90° relative to the photon polarization vector. The photon energy was tuned to the maximum of the dissociative core excited state at 539.2 eV.

0.5th undulator harmonic [37]. The spectra were measured using a high-resolution electron spectrometer SES-2002 (Gammadata-Scienta) equipped with a gas cell. The electron lens axis is in the horizontal direction, at right angles to the photon beam direction [38]. Electron spectra recorded with horizontal and vertical polarization correspond to the photoemission parallel and vertical to the **e** vector, respectively. The monochromator bandpass is ~80 meV full width at half maximum (FWHM), and the electron spectrometer bandpass is ~66 meV FWHM.

The Doppler effect in resonant photoemission was demonstrated for the first time in Ref. [17] for the structures shown here in Fig. 8. In comparison with the spectra shown in that work, the present spectra have been thoroughly analyzed with respect to background contributions and with fittings that were applied on repeated recordings to isolate the Doppler structures.

Figure 8 shows the measured peak corresponding to the decay after excitation with a photon energy of 539.4 eV. The dip on the profile is in qualitative agreement with the simulated profile shown in Fig. 6.

## VII. DISCUSSION

We have presented theory and accompanying *ab initio* wave-packet simulations of resonant photoemission of fixed in space and randomly oriented homonuclear diatomic molecules. Our theory clearly demonstrates the strict parity selection rules in the region of dissociation. These selection rules are related to interchannel interference. The spectral shapes of atomic peaks of fixed in space molecules are strongly asymmetrical in the common case when the potential surfaces of the core excited and final states are nonparallel. This asymmetry can be used for mapping of the potential surfaces. The profile of the atomic peak of fixed in space molecules differ qualitatively for parallel and perpendicular ejection of the Auger electron due to the electronic Doppler effect. We found that the energy position of the atomic peak of fixed in space molecules depends on the lifetime of the core excited state when the molecule has no time to reach the ''strict'' region of dissociation. This shift of the atomic peak is related to the deviation of the potential value at the ''point'' of the decay transition and at dissociation. The physical picture of the formation of the atomic peak becomes more complicated when the molecules are randomly oriented. In this case one can see an unusual interplay of the interchannel interference and the Doppler effect. In principle it should give rise to ultrafine structures—dips or peaks—on top of a Doppler broadened band profile measured at 90° with respect to the polarization vector of the incident radiation. The Doppler interference effect studied in the present work is, however, quite elusive due to a few aspects: The interference term which is responsible for this narrow structure is strictly equal to zero for an infinite lifetime of the core excited state, and the narrow structure appears on the top of the Doppler broadened atomic peak only for finite lifetime broadenings of the core excited state in which case the transitions in the molecular region also start to form an atomic peak. This decay in the molecular region evidently results in a broadening of the atomic peak, something that aggravates the establishment of the ultranarrow resonance, in principle narrower than both the lifetime broadening width and the width of the photon function.

Our measurement clearly indicates a distortion or antisymmetrization of atomic peaks, which we interpret as a manifestation of the predicted Doppler interference.

## ACKNOWLEDGMENTS

The authors acknowledge support from the Consortium ''Center of Advanced Molecular Materials''. Professor Nobuhiro Kosugi is acknowledged for providing the potential surface of core excited state used in the present work, and Professor Vincenzo Carravetta, Professor Yi Luo, and Professor Bernd Schimmelpfennig are acknowledged for valuable discussions.

[1] F. Kh. Gel'mukhanov, L. N. Mazalov, and A. V. Kondratenko, Chem. Phys. Lett. **46**, 133 (1977).
[2] W. Eberhardt, in *Applications of Synchrotron Radiation. Springer Series in Surface Sciences*, Vol. 35, edited by W. Eberhardt (Springer-Verlag, Berlin, 1995), p. 203.
[3] F. Gel'mukhanov and H. Ågren, Phys. Rep. **312**, 87 (1999).
[4] J.-E. Rubensson, J. Electron Spectrosc. Relat. Phenom. **110**, 135 (2000).
[5] S. L. Sorensen and S. Svensson, J. Electron Spectrosc. Relat. Phenom. **114**, 1 (2001).
[6] P. Morin and I. Nenner, Phys. Rev. Lett. **56**, 1913 (1986).
[7] M. Magnuson, J. Guo, C. Såthe, J.-E. Rubensson, J. Nordgren, P. Glans, L. Yang, P. Sałek, and H. Ågren, Phys. Rev. A **59**, 4281 (1999).
[8] P. Erman, A. Karawajczyk, E. Rachlew-Källne, J. Rius i Riu, M. Stankiewicz, K. Yoshiki Franzén, and L. Veseth, Phys. Rev. A **60**, 426 (1999).
[9] A. Karawajczyk, P. Erman, E. Rachlew-Källne, J. Rius i Riu, M. Stankiewicz, K. Yoshiki Franzén, and L. Veseth, Phys. Rev. A **61**, 032718 (2000).
[10] H. Ågren, F. Gel'mukhanov, and P. Sałek, J. Jpn. Soc. Synchrotron Rad. Res. **12**, 257 (1999).
[11] G. B. Armen, H. Aksela, T. Åberg, and S. Aksela, J. Phys. B **33**, 49 (2000).
[12] M. N. Piancastelli, J. Electron Spectrosc. Relat. Phenom. **107**, 1 (2000).
[13] P. Sałek, F. Gel'mukhanov, and H. Ågren, Phys. Rev. A **59**, 1147 (1999).
[14] R. Feifel, F. Burmeister, P. Sałek, M. N. Piancastelli, M. Bäßler, S. L. Sorensen, C. Miron, H. Wang, I. Hjelte, O. Björneholm, A. Naves de Brito, F. Kh. Gel'mukhanov, H. Ågren, and S. Svensson, Phys. Rev. Lett. **85**, 3133 (2000).
[15] P. Sałek, V. Carravetta, F. Kh. Gel'mukhanov, and H. Ågren, J. Chem. Phys. **116**, 629 (2002).
[16] F. Gel'mukhanov, H. Ågren, and P. Sałek, Phys. Rev. A **57**, 2511 (1998).
[17] O. Björneholm, M. Bässler, A. Ausmees, I. Hjelte, R. Feifel, H. Wang, C. Miron, M. N. Piancastelli, S. Svensson, S. L. Sorensen, F. Gel'mukhanov, and H. Ågren, Phys. Rev. Lett. **84**, 2826 (2000).
[18] O. Björneholm, J. Chem. Phys. **115**, 4139 (2001).
[19] L. Rosenqvist, K. Wiesner, A. Naves de Brito, M. Bässler, R. Feifel, I. Hjelte, C. Miron, H. Wang, M. N. Piancastelli, S. Svensson, O. Björneholm, and S. L. Sorensen, J. Chem. Phys. **115**, 3614 (2001).
[20] K. Wiesner, A. Naves de Brito, S. L. Sorensen, F. Burmeister, M. Gisselbrecht, S. Svensson, and O. Björneholm, Chem. Phys. Lett. **354**, 382 (2002).
[21] M. Kitajima *et al.* (to be published).
[22] P. Sałek, F. Gel'mukhanov, H. Ågren, O. Björneholm, and S. Svensson, Phys. Rev. A **60**, 2786 (1999).
[23] P. Sałek, F. Gel'mukhanov, T. Privalov, and H. Ågren, Chem. Phys. Lett. **328**, 425 (2000).
[24] F. Gel'mukhanov and H. Ågren, Pis'ma Zh. Eksp. Teor. Fiz. **67**, 1005 (1998) [JETP Lett. **67**, 1064 (1998)].
[25] P. Morin, M. Simon, C. Miron, N. Leclercq, E. Kukk, J. D. Bozek, and N. Berrah, Phys. Rev. A **61**, 050701 (2000).
[26] F. Gel'mukhanov, P. Sałek, T. Privalov, and H. Ågren, Phys. Rev. A **59**, 380 (1999).
[27] F. Gel'mukhanov and H. Ågren, Phys. Rev. A **49**, 4378 (1994).
[28] F. Gel'mukhanov, V. Carravetta, and H. Ågren, Phys. Rev. B **58**, 2216 (1998).
[29] L. D. Landau and E. M. Lifshitz, *Quantum Mechanics-Nonrelativistic Theory* (Pergamon, London, 1958).
[30] T. Helgaker, H. J. Aa. Jensen, P. Jørgensen, J. Olsen, K. Ruud, H. Ågren, T. Andersen, K. L. Bak, V. Bakken, O. Christiansen, P. Dahle, E. K. Dalskov, T. Enevoldsen, H. Heiberg, H. Hettema, D. Jonsson, S. Kirpekar, R. Kobayashi, H. Koch, K. V. Mikkelsen, P. Norman, M. J. Packer, T. Saue, P. R. Taylor, and O. Vahtras, *Dalton, an ab initio electronic structure program, Release 1.0 (1997). See http://www.kjemi.uio.no/software/dalton/dalton.html*.
[31] N. Kosugi, E. Shigemasa, and A. Yagishita, Chem. Phys. Lett. **190**, 481 (1992).
[32] A. Yagishita, E. Shigemasa, and N. Kosugi, Phys. Rev. Lett. **72**, 3961 (1994).
[33] P. Sałek, Comput. Phys. Commun. (to be published).
[34] K. Siegbahn, C. Nordling, G. Johansson, J. Hedman, P. F. Hedén, K. Hamrin, U. Gelius, T. Bergmark, L. O. Werme, R. Manne, and Y. Baer, *ESCA Applied to Free Molecules* (North-Holland, Amsterdam, 1969).
[35] H. Ohashi *et al.*, Nucl. Instrum. Methods Phys. Res. A **467**, 529 (2001).
[36] H. Ohashi *et al.*, Nucl. Instrum. Methods Phys. Res. A **467**, 533 (2001).
[37] T. Tanaka and H. Kitamura, J. Synchrotron Radiat. **3**, 47 (1996).
[38] Y. Shimizu *et al.*, J. Electron Spectrosc. Relat. Phenom. **114**, 63 (2001).